A Computational Model of Red Blood Cell Dynamics in Patients with Chronic Kidney Disease

H. T. Banks[1], Karen M. Bliss[1], Peter Kotanko[2], Hien Tran[1]

[1]Center for Research in Scientific Computation, North Carolina State University
[2]Renal Research Institute, New York

February 15, 2011

Abstract

Kidneys are the main site of production of the hormone erythropoietin (EPO) that is the major regulator of erythropoiesis, or red blood cell production. EPO level is normally controlled by a negative feedback mechanism in the kidneys, but patients with chronic kidney disease (CKD) do not produce sufficient levels of EPO to maintain appropriate blood hemoglobin concentration. A mathematical model, including interactions with iron and inflammation, is developed for erythropoiesis in patients with CKD. Numerical solution methodologies and validation of numerical results are discussed. Simulation results under varying conditions and treatment protocols are presented.

Further author information: (Send correspondence to Karen M. Bliss.)

Karen M. Bliss: kmbliss@ncsu.edu
H. T. Banks: htbanks@ncsu.edu
Peter Kotanko: pkotanko@rriny.com
Hien Tran: tran@ncsu.edu

1 Introduction

It is estimated that 31 million Americans have chronic kidney disease (CKD). Among those, approximately 330 thousand are classified as being in End-Stage Renal Disease (ESRD) and require dialysis [17]. Dialysis is the bidirectional exchange of materials across a semipermeable membrane [2]. For the purposes of this study, we consider only hemodialysis, where a patient's blood is exposed to a semipermeable membrane outside of the body.

In addition to regulating blood pressure and filtering waste products from blood, kidneys produce a hormone called erythropoietin (EPO) that is the major regulator of erythropoiesis, or red blood cell production. EPO level is normally controlled by a negative feedback mechanism in the kidneys, but patients in ESRD do not produce sufficient levels of EPO to maintain blood hemoglobin concentration. Hemoglobin is the protein that gives red blood cells the ability to carry oxygen. Patients with low hemoglobin concentration may present symptoms of anemia, such as decreased cardiac function, fatigue, and decreased cognitive function.

In order to prevent anemia, patients typically receive recombinant human EPO (rHuEPO) intravenously to stimulate red blood cell production. However, treatment is far from perfect. In 2006, only half of dialysis patients had a mean monthly hemoglobin greater than 11 grams per deciliter [17], the desired minimum level set by the National Kidney Foundation [13].

Iron is required to produce hemoglobin, and iron deficiency can be an issue among patients receiving rHuEPO therapy. Oral iron supplementation is often ineffective, so intravenous iron supplementation has become a mainstay in many patients undergoing rHuEPO therapy [9].

Iron availability is negatively affected by inflammation level in the body. Most patients with CKD have elevated levels of inflammation due to CKD and the presence of other medical issues (e.g., diabetes, hypertension, etc.) [10].

Our goals are (1) the development of a mathematical model for erythropoiesis of patients in ESRD undergoing hemodialysis, taking into consideration the effects of EPO, iron level, and inflammation level in the body, which has a reasonable degree of fidelity to the biological system, and (2) the development of model-based control of the system. This note is a step toward the first of these two goals.

2 Erythropoiesis

Erythropoiesis is the process by which erythrocytes, or red blood cells (RBCs), are formed. Erythrocytes transport oxygen and carbon dioxide between the lungs and all of the tissues of the body and can be thought of as a container for hemoglobin [15], the protein that carries oxygen.

Erythrocytes are produced primarily from pluripotent stem cells in bone marrow. In the presence of the cytokine named stem cell factor, hematopoietic stem cells divide asymetrically, producing a committed colony-forming-unit (CFU) while maintaining the population of stem cells. The erythrocyte lineage shares the precursor CFU-GEMM (granulocyte, erythrocyte, macrophage, megakaryocyte) with other types of blood cells (white blood cells, platelets, etc.). The exact mechanisms determining selection of lineage from this nodal point are not known [6].

Erythrocyte lineage continues as described in Figure 1: erythroid burst-forming unit (BFU-E), erythroid colony-forming-unit (CFU-E), proerythrocyte, basophilic erythrocyte, polychromatic erythroblast, orthochromatic erythroblast, reticulocyte, and erythrocyte. Cell division ceases with the formation of the orthochromatic erythroblast. Division rate, death rate, and maturation rate are influenced by the level of EPO [6]. This is described in more detail later.

Hemoglobin is synthesized beginning in the CFU-E stage, with the majority of synthesis occurring

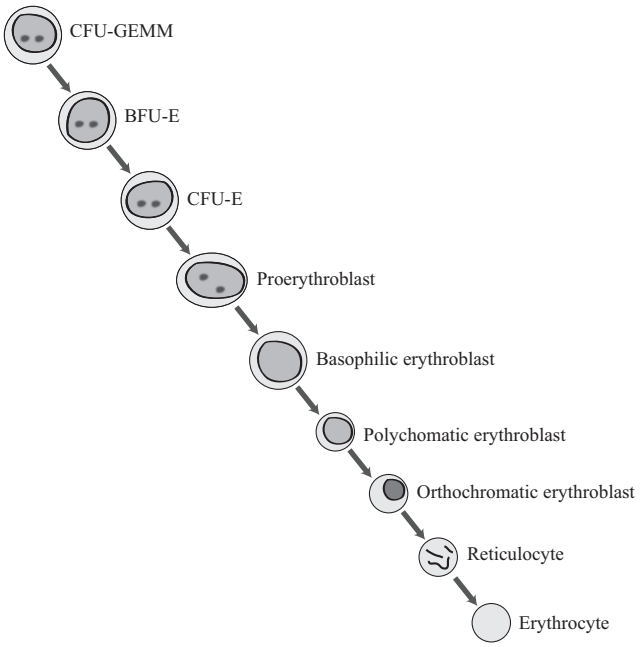

Figure 1: Erythropoiesis cell lineage.

in the polychromatic erythroblast stage. When the nucleus is extruded from the cell, the cell is named a reticulocyte. Little hemoglobin synthesis happens at the reticulocyte stage, and synthesis is completely absent in mature erythrocytes [6].

Reticulocytes begin to lose the adhesive proteins that hold them in the bone marrow. They decrease in size and begin to circulate in the blood. In healthy individuals, the time from proerythroblast to mature erythrocyte is approximately 7 days. Normal erythrocyte life span is approximately 120 days, at which time aging erythrocytes are enveloped by macrophages in the spleen.

3 Previous models

The process of erythropoiesis has been modeled in many physiological scenarios. In [14], rHuEPO therapy is considered in healthy volunteers. This model incorporates the negative feedback to endogenous EPO production. EPO is assumed to be cleared using Michaelis-Menten dynamics. A similar model was used to fit data in rats [18]. Both of these models use delay instead of age-structured modeling.

Both [3] and [4] use age-structured models, as does the model described in [11], which assumes that the oldest mature erythrocytes will be destroyed, yielding a moving boundary condition. In [1], EPO is assumed to accelerate maturation of cells undergoing erythropoiesis. Additionally, EPO is assumed to be consumed during the process of erythropoiesis.

The model presented here is a significant departure from these models in that it incorporates the effects of both iron plasma level and inflammation.

4 Model Overview

We use an age-structured model with three major classifications of erythroid cells in which the structure variables μ, ν, and ψ represent maturity levels, as shown in Figure 2.

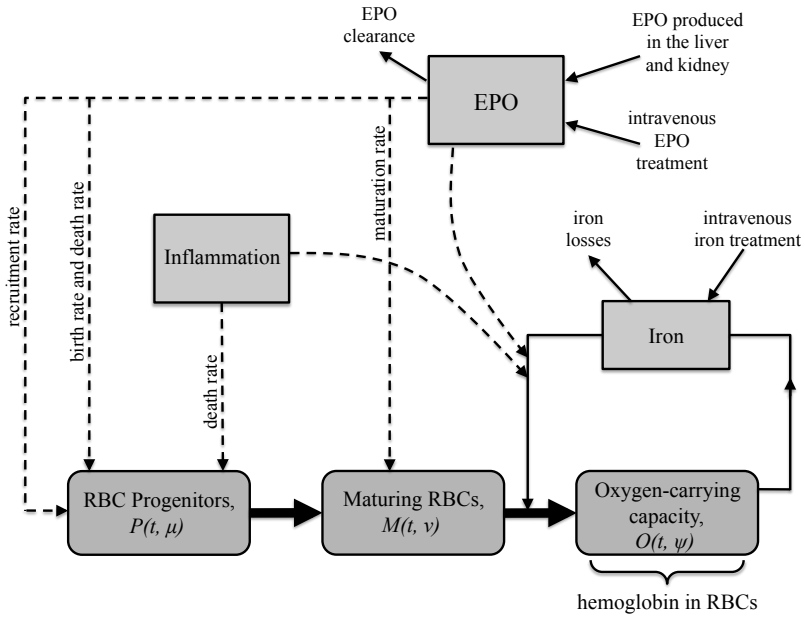

Figure 2: Model schematic.

$P(t,\mu)$ and $M(t,\nu)$ represent the number of progenitor cells and maturing hematopoietic cells, respectively. $O(t,\psi)$ is a measure of the oxygen carrying capacity of circulating reticulocytes and erythrocytes. For these cell classes, the second argument (e.g., μ for class P) is the structure variable, maturity level in this case. We model EPO level, E, iron level, Fe, and a measure of overall inflammation in the body, I. Time is measured in days.

Our state variables are

$$P = P(t,\mu), \quad M = M(t,\nu), \quad O = O(t,\psi), \quad E = E(t), \text{ and } Fe = Fe(t).$$

Rate of exogenous EPO treatments, $\dot{E}_{ex}$, and rate of exogenous iron treatments, $\dot{Fe}_{ex}$, are input functions, and hemoglobin concentration, $Hb(t)$, is the output of the model.

We will make use of sigmoid functions throughout the model. An increasing sigmoid function will be of the form

$$F(x) = \left(F^{min} - F^{max}\right) \cdot \frac{c^k}{c^k + x^k} + F^{max}.$$

Note that when x is small, $F(x)$ is close to F^{min}, and when x is large, $F(x)$ is close to F^{max}. The typical graph of such a function is depicted in Figure 3a. The values of c and k affect the slope of the curve and the location of the area of increase.

Similarly, a typical decreasing sigmoid function is depicted in Figure 3b and has the form

$$G(x) = \left(G^{max} - G^{min}\right) \cdot \frac{c^k}{c^k + x^k} + G^{min}.$$

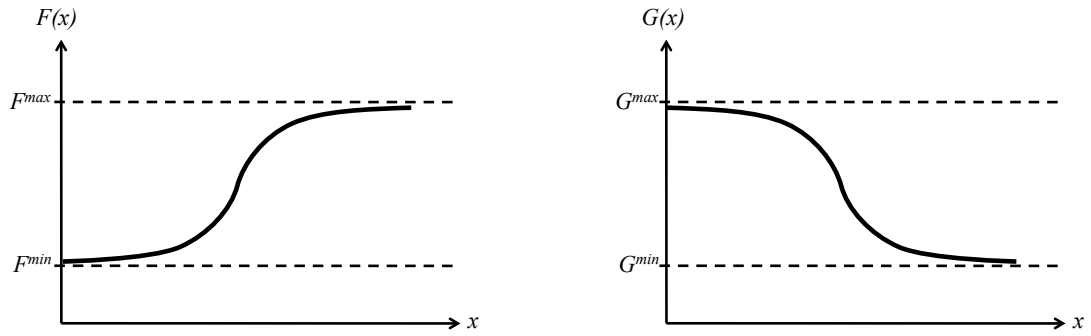

(a) Generic increasing sigmoid function.

(b) Generic decreasing sigmoid function.

Figure 3: Sigmoid function examples.

5 Iron

Iron is required to make hemoglobin, the protein that gives erythrocytes the ability to carry oxygen. It is also the protein that gives erythrocytes their characteristic red color. If iron is not available during erythropoiesis, the result is lighter-colored (hypochromic) erythrocytes with reduced capacity to carry oxygen.

Control of iron in the body is a strictly regulated process, in part because there is no pathway for the excretion of excess iron (Figure 4).

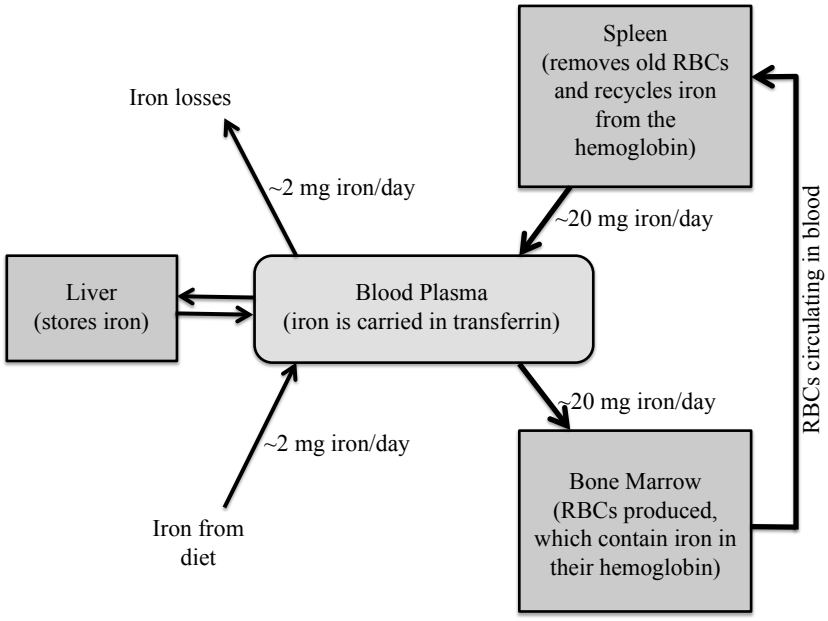

Figure 4: Iron cycle in healthy individuals.

When red blood cells age, they become enveloped by macrophages in the spleen. The iron from their hemoglobin is then recaptured and sent to the bone marrow for use in making hemoglobin for new erythrocytes. This recycling process is very efficient and is the main source of iron to erythropoiesis [15]. In much smaller quantities, iron is absorbed from diet in the duodenum and can be stored in the liver. The only losses to the system are from sweating, cells being shed, blood losses, etc.

Iron is stored in the compound ferritin when it is within a cell, and in the compound transferrin when it is in the blood plasma. The protein ferroportin is required to transport iron out of a cell and into the plasma. The major regulator of this transport is the hormone hepcidin, which is produced in the liver. Hepcidin binds to ferroportin and causes the complex to be absorbed into the cell, effectively interrupting the transport of iron into the blood plasma, as depicted in Figure 5.

Hepcidin production is increased in the presence of certain cytokines which are released due to inflammation in the body. It is thought that this might be a defense mechanism against foreign organisms which may need iron to reproduce.

Since patients in ESRD commonly have other health problems (such as diabetes and hypertension), they often have higher than normal levels of inflammation. Thus, they may produce higher than normal levels of hepcidin. As a result, even if there is enough iron in the body, it may not be available for erythropoiesis because it cannot leave the cells and enter the plasma.

Current research suggests that EPO affects the interaction between cytokines and hepcidin. When EPO level is sufficiently high, the effects of inflammation cannot be seen.

We model the amount, Fe, of iron in the blood plasma, in milligrams. We formulate a mass balance involving the iron compartment (see Figure 6) as follows.

The main source of incoming iron to the compartment is recycled iron from the hemoglobin of senescent erythrocytes that are enveloped by macrophages. We will develop class O so that each member in the class is assumed to contain exactly the same amount of iron. That is, the rate of iron being recycled from class O is $k_{Fe}\int_0^{\psi_f}\delta_O(\psi)O(t,\psi)\partial\psi$, where k_{Fe} is some proportionality constant and $\delta_O(\psi)$ is the death rate of the cells in class O, explained in more detail later.

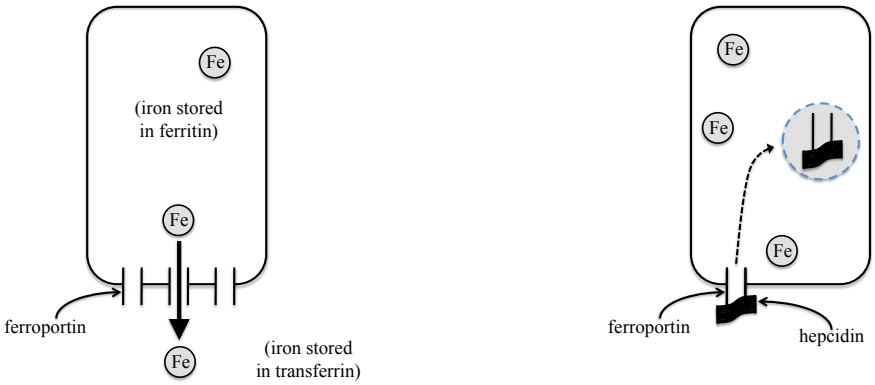

(a) Ferroportin is required for the transport of iron out of cells.

(b) Hepcidin is the major regulator of iron transport out of cells.

Figure 5: Iron regulation at a cellular level.

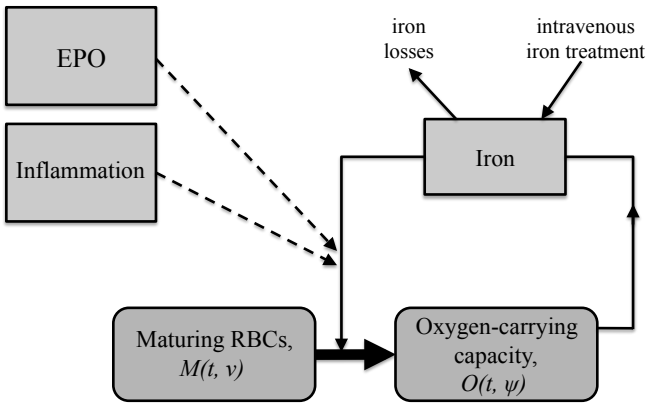

Figure 6: Iron compartment.

The other main source of iron to the compartment is exogenous iron supplied as part of treatment. We denote the rate of exogenous iron treatment by $\dot{Fe}_{ex}(t)$

A small amount of iron enters the system through absorption from diet and from storage in the liver, and there are also iron losses (due to sweating, blood losses during blood draws and hemodialysis, etc.). As described earlier, patients undergoing hemodialysis require iron supplements intravenously. Therefore we assume that when we sum the iron losses and the iron entering the system from diet and storage in the liver we obtain a net loss. Further, we will assume for an initial model that the loss occurs at constant rate unless the current level of iron is small, in which case a fraction of the iron is lost. That is, that rate of iron loss, $\rho_{Fe,loss}(Fe)$, is given by

$$\rho_{Fe,loss}(Fe) = \begin{cases} \rho_{Fe,const}, & Fe \geq Fe_{th} \\ \rho_{Fe,frac} \cdot Fe, & Fe < Fe_{th}. \end{cases}$$

This assumption will be revisited in future models, perhaps with greater losses when dialysis and blood draws occur.

Next we need to account for iron leaving the compartment during erythropoiesis. For our first model, we begin by making the assumption that iron enters red blood cells at the moment that a cell matures from class M to class O, which is the time that a cell leaves the bone marrow and begins circulating. Red blood cells actually collect iron over the time period that they are in class M, but the biochemistry of this process is not clearly understood. The assumption that all of the iron is collected into a cell at one moment will certainly have to be revisited in future improvements of the model.

In determining the amount of iron used during erythropoiesis, we first compute the amount of iron that would be used if every cell leaving class M were to contain the appropriate amount of hemoglobin so as to be at full oxygen-carrying capacity, i.e.,

$$Fe_{needed} = k_{Fe} M(t, \nu_f). \tag{1}$$

In the presence of inflammation, even if there is enough iron in the plasma, it may not be available to be used in erythropoiesis. For our initial model, we assume that there is an EPO threshold, EPO_{th}.

We assume that if EPO is above the threshold, the effects of inflammation can not be seen. That is, we assume

$$Fe_{avail} = k_{Fe,eff} f(E, I) Fe, \tag{2}$$

where

$$f(E,I) = \begin{cases} \dfrac{(c_{Fe,av})^{k_{Fe,av}}}{(c_{Fe,av})^{k_{Fe,av}} + I^{k_{Fe,av}}}, & E < EPO_{th} \\ 1, & E \geq EPO_{th}. \end{cases}$$

Observe that in this model when EPO is greater than the threshold level, inflammation level does not impact iron availability. However, when EPO level is lower than the threshold, the amount of available iron depends on inflammation level–as $f(E, I)$ is close to one when inflammation is low and close to zero when inflammation is high. The constant $k_{Fe,eff}$, with $0 \leq k_{Fe,eff} \leq 1$, is an efficacy constant that accounts for the fact that only a fraction of the iron in the plasma will actually be available at the site of erythropoiesis at any given time.

The amount of iron actually used in erythropoiesis is therefore given by

$$\begin{aligned} Fe_{used} &= \min\left\{Fe_{needed},\ Fe_{avail}\right\}, \\ &= \min\left\{k_{Fe} M(t, \nu_f),\ k_{Fe,eff} f(E, I) Fe\right\}. \end{aligned} \tag{3}$$

We assume that the rate of iron leaving the iron compartment and entering class O is proportional to this quantity, Fe_{used}. That is,

$$\rho_{Fe \to O} = k_{\rho,Fe} Fe_{used}.$$

Thus, the mass balance in the iron compartment is given by

$$\begin{aligned} \dot{Fe}(t) &= (\text{rate in from class } O) + (\text{rate in intravenously}) \\ &\qquad - (\text{rate out to class } O) - (\text{rate of iron losses}) \\ &= k_{Fe} \int_0^{\psi_f} \delta_O(\psi) O(t, \psi) d\psi + \dot{Fe}_{ex}(t) - \rho_{Fe \to O} - \rho_{Fe,loss}(Fe). \end{aligned} \tag{4}$$

6 EPO

EPO is the primary regulator of erythropoiesis. It stimulates red blood cell production, differentiation and maturation, and prevents apoptosis [6]. In healthy individuals, the majority of EPO production occurs in the kidney. Sensors in the kidney monitor blood oxygen level. EPO production is increased in response to low oxygen level and is decreased when oxygen level is high.

Patients in ESRD, whose kidneys have only minimal function, produce only a small basal level of EPO in the kidney and liver [7]. Without intervention, patients can develop anemia; therefore, patients undergoing dialysis are commonly treated with intravenous rHuEPO. Two common rHuEPOs, epoetin alfa and epoetin beta, share structural homology with endogenous EPO. Darbepoietin alfa, the other major erythropoietic agent, is designed so that it has a longer half-life *in-vivo.* In this model, we assume that darbepoietin is not the erythropoietic agent, and therefore we will not distinguish between rHuEPO and endogenous EPO with respect to their action. We assume that their effects on erythropoiesis are identical.

EPO is measured in units of EPO. We assume the rate of endogenous EPO production in the liver and kidney to be constant, and will denote it $\rho_{EPO,basal}$.

We will assume that EPO clearance is proportional to the amount present, although we could consider Michaelis-Menten dynamics in future models. Finally, we also account for the rate of EPO given via IV, denoted $\dot{E}_{ex}(t)$. So we have

$$\dot{E}(t) = \rho_{EPO,basal} + \dot{E}_{ex}(t) - \frac{1}{t_{1/2}} \ln 2 \cdot E(t),$$

where $t_{1/2}$ is the half-life of EPO.

7 Inflammation

Inflammation affects two aspects of erythropoiesis, as depicted in Figure 2.

Even in patients without CKD, chronic inflammation can cause anemia, termed the anemia of chronic disease. While the exact chemical pathways are not necessarily known, it is known that the presence of inflammation can suppress erythropoiesis and may inhibit the action of EPO [16]. Since EPO affects the birth and death rate of progenitors, we incorporate inflammation in the death rate term associated with the progenitor cell class, P.

Inflammation level also impacts iron availability for erythropoiesis, as described previously. Inflammation may cause an increase in ferritin production, which would cause iron to be retained within cells, inhibiting the use of iron to make hemoglobin. Inflammation may also impair the ability of the body to absorb dietary iron [16].

It is almost certain that inflammation affects these two aspects of erythropoiesis via completely different chemical pathways. We assume that both aspects can be sufficiently described with some overall measure of inflammation in the body. There are markers of inflammation, such as albumin and C-reactive protein, which are often measured in patients undergoing dialysis. In future work, we will investigate whether inflammation can be described as some combination of the levels of these markers.

8 Class $P(t, \mu)$

We group the progenitor cells (CFU-GEMM, BFU-E and CFU-E) in one class, $P(t, \mu)$. These cells are affected by EPO level and inflammation level.

We make the following assumptions:

(i) There is a smallest maturity level, $\mu_0 = 0$, and a largest maturity level, μ_f; i.e., $0 \leq \mu \leq \mu_f$.

(ii) The maturity rate depends on the EPO concentration and the maturity level [6]. For simplification in our initial model, we assume that the maturity rate is constant:

$$\frac{d\mu}{dt} = \rho_P.$$

(iii) The birth rate depends on EPO concentration [6] and the maturity level.

Regulation of erythropoiesis by EPO is focused on the progenitor class, and probably most importantly the CFU-E. A rise in EPO level results in proliferation of CFU-E [6]. We will

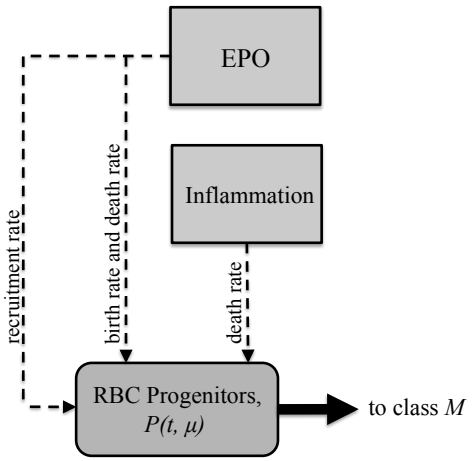

Figure 7: The progenitor cells, $P(t, \mu)$.

assume EPO affects all cells in class P equally, independent of maturity level. We will model the birth rate as an increasing sigmoid function,

$$\beta_P(E) = \left(\beta_P^{min} - \beta_P^{max}\right) \frac{(c_{\beta,P})^{k_{\beta,P}}}{(c_{\beta,P})^{k_{\beta,P}} + E^{k_{\beta,P}}} + \beta_P^{max}.$$

(iv) The number of stem cells being recruited into the precursor cell population is directly proportional to EPO level:

$$P(t, 0) = R_P E(t).$$

It is reasonable to assume that recruitment is related to EPO level, as it is one of the hormones that affects whether a stem cell will become an erythrocyte. Other hormones are certainly involved as well, but the chemical pathway governing the differentiation of stem cells is still largely unknown [6].

(v) The death rate depends on the concentration of EPO, the inflammation level, and the maturity level, μ. We will simplify this for our first model to assume that death rate is not dependent on maturity level.

EPO prevents apoptosis, or programmed cell death, of progenitor cells [6]. We use a decreasing sigmoid function to describe this behavior.

Certain interferons, present under inflammatory conditions, can also cause death of progenitor cells, specifically CFU-E [12]. We assume that the death rate of progenitor cells depends on inflammation level, which is modeled by some increasing sigmoid function.

Finally, we assume that overall death rate is the sum of these two effects:

$$\delta_P(E, I) = \left(\delta_{P,E}^{max} - \delta_{P,E}^{min}\right) \frac{(c_{\delta,P,E})^{k_{\delta,P,E}}}{(c_{\delta,P,E})^{k_{\delta,P,E}} + E^{k_{\delta,P,E}}} + \delta_{P,E}^{min}$$
$$+ \left(\delta_{P,I}^{min} - \delta_{P,I}^{max}\right) \frac{(c_{\delta,P,I})^{k_{\delta,P,I}}}{(c_{\delta,P,I})^{k_{\delta,P,I}} + I^{k_{\delta,P,I}}} + \delta_{P,I}^{max}.$$

Now we consider the rate of change in population from maturity level μ to maturity level $\mu + \Delta\mu$.

rate of change in population on the interval $(\mu, \mu + \Delta\mu) =$
(rate of cells entering the interval) − (rate of cells leaving the interval)
+ (birth rate term) − (death rate term)

$$\frac{\partial}{\partial t}\int_{\mu}^{\mu+\Delta\mu} P(t,\xi)d\xi = \rho_P P(t,\mu) - \rho_P P(t,\mu+\Delta\mu) + \int_{\mu}^{\mu+\Delta\mu} \beta_P(E)\, P(t,\xi)d\xi - \int_{\mu}^{\mu+\Delta\mu} \delta_P(E,I)P(t,\xi)d\xi$$

$$\frac{\partial}{\partial t}\int_{\mu}^{\mu+\Delta\mu} P(t,\xi)d\xi = -\rho_P\left[P(t,\mu+\Delta\mu) - P(t,\mu)\right] + \left[\beta_P(E) - \delta_P(E,I)\right]\int_{\mu}^{\mu+\Delta\mu} P(t,\xi)d\xi$$

Dividing by $\Delta\mu$ and then letting $\Delta\mu \to 0$, we obtain

$$\frac{\partial}{\partial t}P(t,\mu) = -\rho_P\frac{\partial}{\partial \mu}P(t,\mu) + \left[\beta_P(E) - \delta_P(E,I)\right]P(t,\mu),$$

and we have the boundary condition

$$P(t,0) = R_P E(t).$$

9 Class $M(t,\nu)$

Class $M(t,\nu)$ consists of immature hematopoietic cells: proerythroblasts, basophilic erythroblasts, polychromatic erythroblasts, orthochromatic erythroblasts, and non-circulating reticulocytes (i.e. those that still reside in the bone marrow). Cells are recruited from class P and, upon maturation, feed into class O. Their development is influenced by EPO concentration.

We make the following assumptions:

(i) There is a smallest maturity level, $\nu_0 = 0$, and a largest maturity level, ν_f. That is, $0 \le \nu \le \nu_f$.

(ii) The maturation rate depends on the level of erythropoietin and the maturity level. However, for our initial model, we assume that maturation rate *does not* depend on the maturity level.

EPO stimulates maturation [6], so we use an increasing sigmoid function for maturation rate, $\rho_M(E)$.

$$\rho_M(E) = \left(\rho_M^{min} - \rho_M^{max}\right)\frac{(c_{\rho,M})^{k_{\rho,M}}}{(c_{\rho,M})^{k_{\rho,M}} + E^{k_{\rho,M}}} + \rho_M^{max}.$$

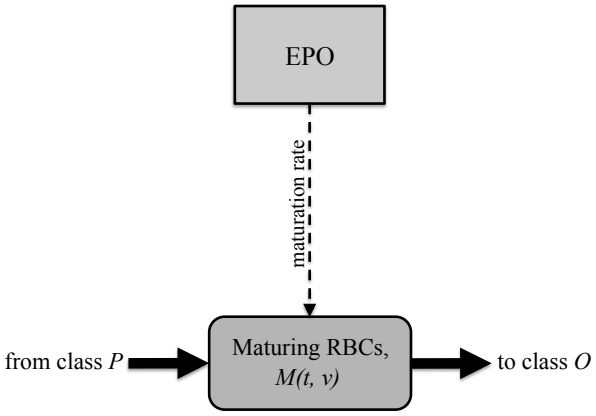

Figure 8: Maturing erythrocytes, $M(t, \nu)$.

(iii) The birth rate depends on the maturity level, but for our first model, we assume birth rate is a constant, $\tilde{\beta}_M$.

(iv) The number of cells at maturity level $\nu = 0$ is equal to the number of cells leaving the previous stage:

$$M(t, 0) = P(t, \mu_F).$$

(v) The death rate depends on the maturity level, ν and on the iron level. To simplify, we assume the death rate is a constant, δ_M.

As in the progenitor class, we can consider the rate of change in population from maturity level ν to maturity level $\nu + \Delta\nu$, then divide by $\Delta\nu$ and let $\Delta\nu \to 0$ to obtain

$$\frac{d}{dt}M(t, \nu) = -\rho_M(E)\,\frac{\partial}{\partial \nu}M(t, \nu) + \left[\tilde{\beta}_M - \delta_M\right] M(t, \nu).$$

Since we have made the assumption that the birth and death rates are both constant, it is clear that they will not both be identifiable. We replace the difference $\tilde{\beta}_M - \delta_M$ by the constant β_M, which then represents the net birth rate.

Hence, we have

$$\frac{\partial}{\partial t}M(t, \nu) = -\rho_M(E)\,\frac{\partial}{\partial \nu}M(t, \nu) + \beta_M M(t, \nu),$$

with the boundary condition

$$M(t, 0) = P(t, \mu_F).$$

It is worth noting again that as this is our first model of the system, we have made the assumption that iron level does not impact cell development until cells mature out of class M into class O. Specifically, we do not account for iron entering red blood cells throughout class M and we ignore any impact this would have on death rate in class M. Future versions of the model will need to account for these interactions with the iron compartment.

10 Class O

Unlike the classes P and M, class O does not represent *the number* of circulating reticulocytes and mature erythrocytes, because knowledge of the number of cells alone does not give us enough information to determine whether the cells contain the necessary amount of hemoglobin to carry oxygen at full capacity.

Erythrocytes begin hemoglobinization at the polychromatic erythroblast stage (in class M). They continue to acquire more hemoglobin throughout the orthochromatic erythroblast stage and into the reticulocyte stage, until the reticulocyte leaves the bone marrow, at which time it ceases hemoglobinization [15]. Hence, the oxygen carrying ability of a mature erythrocyte is determined by how much hemoglobin is available during the time interval when that cell is in class M.

In order to initially simplify computations, we assume that a cell's oxygen-carrying ability is based solely on the availability of iron at the time that the cell matures out of class M and begins circulating in the blood. As previously noted, the biology does not support this formulation of the problem, and this assumption will be reconsidered in future models.

Let us consider an example in order to elucidate this idea. Suppose we know that $k_{Fe} = 0.2$ mg/billion cells and that at some given time t, $Fe_{avail} = 8$ mg. Suppose also that at time t there are 100 billion cells maturing out of class M; that is, $M(t, \nu_f) = 100$. Then

$$Fe_{avail} < Fe_{needed} = k_{Fe} M(t, \nu_f) = 20 \text{ mg}.$$

Then, per equation (3), $Fe_{used} = Fe_{avail} = 8$ mg, which is only 40% of the 20 mg that would be needed for each cell maturing into class O to have full oxygen-carrying capacity. Then the 100 billion cells maturing into class O would have, on average, only 40% oxygen-carrying ability. It would be difficult to track both the number of circulating erythroid cells and the oxygen carrying capacity of each. Instead, we think of the 100 billion cells with 40% oxygen-carrying ability as 40 billion cells with 100% oxygen-carrying capacity. Hence, every "cell" in class O is assumed to have full-oxygen carrying capacity.

Now we present the assumptions we make about class O.

(i) We assume that there is a smallest maturity level, $\psi_0 = 0$, and a largest maturity level, ψ_f. That is, $0 \leq \psi \leq \psi_f$. In the future, we may wish to allow ψ_f to vary.

(ii) The maturation rate of cells in this class is a function of the maturity level. We will further assume, for simplification in this initial model, that the maturity rate is constant:

$$\frac{d\psi}{dt} = \rho_O$$

(iii) The birth rate is zero. Cells at this stage mature but do not proliferate [6].

(iv) The number of members of class O at maturity level $\psi = 0$ is equal to the number of cells leaving the previous stage multiplied by the ratio of Fe_{used} and Fe_{needed}:

$$\begin{aligned} O(t,0) &= \frac{Fe_{used}}{Fe_{needed}} \cdot M(t, \nu_f), \\ &= \frac{Fe_{used}}{k_{Fe} M(t, \nu_f)} \cdot M(t, \nu_f), \\ &= \frac{1}{k_{Fe}} Fe_{used}. \end{aligned} \tag{5}$$

As stated above, this assumption guarantees that each member of class O has full oxygen-carrying ability.

(v) The death rate of cells in the class $O(t,\psi)$, depends on the maturity level. We expect this to be an increasing function, because macrophages envelop mainly aging adult erythrocytes [15]. Therefore, we will use the increasing sigmoid function

$$\delta_O(\psi) = \left(\delta_O^{min} - \delta_O^{max}\right) \frac{(c_{\delta,O})^{k_{\delta,O}}}{(c_{\delta,O})^{k_{\delta,O}} + \psi^{k_{\delta,O}}} + \delta_O^{max}.$$

As in classes P and M, we can generate the partial differential equation

$$\frac{\partial}{\partial t}O(t,\psi) = -\rho_O \frac{\partial}{\partial \psi}O(t,\psi) - \delta_O(\psi)O(t,\psi)$$

with boundary condition (5).

11 Hemoglobin Concentration

We have already assumed that hemoglobin exists only in erythrocytes in class O. We compute the total number of members in class O at a given time t by

$$\int_0^{\psi_f} O(t,\psi)d\psi. \tag{6}$$

We previously made the assumption that each member of class O has exactly the same amount of iron. Specifically, if we multiply the quantity (6) by k_{Fe}, we have the amount of iron (in mg) circulating in erythrocytes at time t. We then multiply by a conversion factor to find the amount of hemoglobin circulating. Then we need only divide by blood volume, $BV(t)$, to determine the hemoglobin concentration.

Blood volume is difficult to determine and varies greatly in patients undergoing dialysis. Patients in ESRD are unable to clear fluids from their bodies. Fluids, for the most part, build up in the patient's body between dialysis treatments. Therefore, we assume that blood volume increases linearly between dialysis treatments and decreases linearly during a dialysis treatment. Initially we simulate patients undergoing dialysis (1) three times per week (i.e. Monday-Wednesday-Friday, or MWF), or (2) every third day (ETD), as in Figure 9.

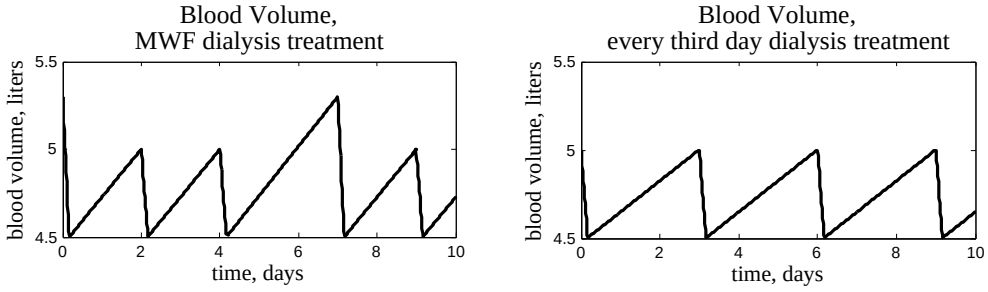

Figure 9: Blood volume over various treatment protocols.

Hence, hemoglobin concentration is a nonlinear function of the amount of iron circulating,

$$Hb(t) = \frac{k_{Fe}\int_0^{\psi_f} O(t,\psi)d\psi}{BV(t)}.$$

12 Modification to the Model

We now discuss how we produce a smooth approximation to the piecewise-defined function

$$f(E,I) = \begin{cases} f_{E<EPO_{th}}, & E < EPO_{th} \\ 1, & E \geq EPO_{th} \end{cases}$$

where

$$f_{E<EPO_{th}} = \frac{(c_{Fe,av})^{k_{Fe,av}}}{(c_{Fe,av})^{k_{Fe,av}} + I^{k_{Fe,av}}}.$$

For our initial simulations, we assume that inflammation remains constant. Hence, for a given inflammation level, f is a step function that oscillates between 1 and the constant $0 \leq f_{E<EPO_{th}} \leq 1$.

Rather than choose the constants $c_{Fe,av}$ and $k_{Fe,av}$, we choose two parameters $0 < f_1, f_{0.5} < 1$ such that when $E < EPO_{th}$,

$$f(E,1) = f_1 \text{ and } f(E,0.5) = f_{0.5}.$$

Thus,

$$\frac{(c_{Fe,av})^{k_{Fe,av}}}{(c_{Fe,av})^{k_{Fe,av}} + 1^{k_{Fe,av}}} = f_1 \tag{7}$$

and

$$\frac{(c_{Fe,av})^{k_{Fe,av}}}{(c_{Fe,av})^{k_{Fe,av}} + (0.5)^{k_{Fe,av}}} = f_{0.5}. \tag{8}$$

Then we solve (7) and (8) for the constants $c_{Fe,av}$ and $k_{Fe,av}$:

$$k_{Fe,av} = \frac{\ln f_{0.5} + \ln(1-f_1) - \ln f_1 - \ln(f_{0.5})}{\ln 2}$$

and

$$c_{Fe,av} = \left(\frac{1}{1-f_1}\right)^{\frac{\ln 2}{\ln f_{0.5} + \ln(1-f_1) - \ln f_1 - \ln(f_{0.5})}}.$$

We solve the EPO differential equation for a given treatment protocol. Then we use the solution to determine times $t_i = t_i(E)$ where EPO moves from above EPO_{th} to below EPO_{th} and vice versa, as in Figure 10.

We approximate f with

$$f^s(E,I,t) = h_{shift} + \sum_i h(i,I)H^s_{t_i}(t),$$

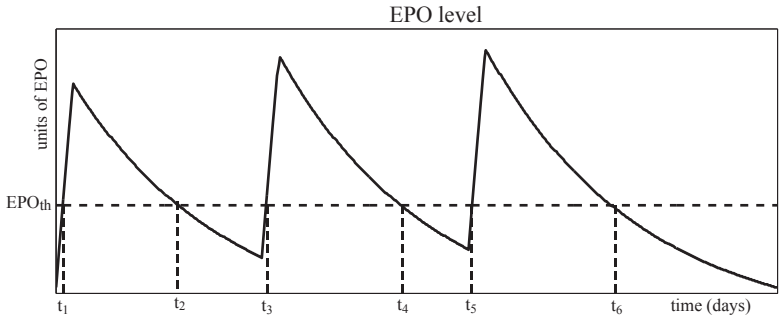

Figure 10: Determining the times t_i where $E(t) = EPO_{th}$.

a linear combination of smoothed "heaviside" functions of the form

$$H^s_{t_i}(t) = \frac{1}{2} + \frac{1}{2}\tanh\left(k_{heavy}(t - t_i)\right)$$
$$= \frac{1}{1 + e^{-2k_{heavy}(t-t_i)}}.$$

Choice of the parameter k_{heavy} determines the steepness of the approximation to each jump discontinuity. The coefficients $h(i, E)$ depend on (i) whether EPO level is passing from above EPO_{th} to below or vice versa, and (ii) the value of the quantity $f_{E<EPO_{th}}$, which depends on the level of inflammation.

Figure 11 shows an example of a function f (EPO three times per week, inflammation =0.5) with two smooth approximations, $k_{heavy} = 15$ and $k_{heavy} = 5$.

This formulation yields a function f^s that is smooth, approximates f, and has a smooth derivative. We replace f with f^s throughout the model and therefore we use the parameters f_1, $f_{0.5}$ and k_{heavy} in place of $c_{Fe,av}$ and $k_{Fe,av}$.

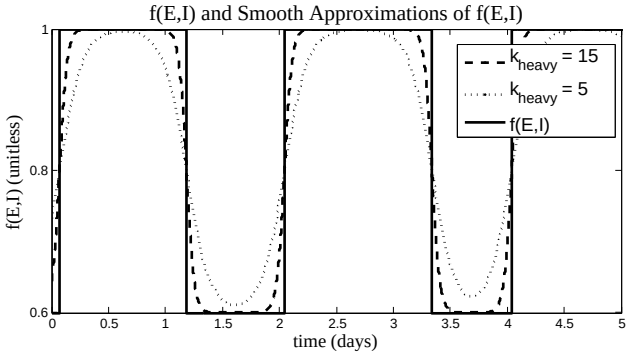

Figure 11: A smooth approximation of the function $f(E, I)$.

13 Model Summary

In summary, we have the system

$$\frac{\partial}{\partial t}P(t,\mu) = -\rho_P \frac{\partial}{\partial \mu}P(t,\mu) + \left[\beta_P(E) - \delta_P(E,I)\right] P(t,\mu), \tag{9}$$

$$\frac{\partial}{\partial t}M(t,\nu) = -\rho_M(E)\,\frac{\partial}{\partial \nu}M(t,\nu) + \beta_M M(t,\nu), \tag{10}$$

$$\frac{\partial}{\partial t}O(t,\psi) = -\rho_O \frac{\partial}{\partial \psi}O(t,\psi) - \delta_O(\psi)O(t,\psi), \tag{11}$$

$$\dot{Fe}(t) = k_{Fe}\int_0^{\psi_f} \delta_O(\psi)O(t,\psi)d\psi + \dot{Fe}_{ex}(t) - \rho_{Fe\to O} - \rho_{Fe,loss} \tag{12}$$

$$\dot{E}(t) = \rho_{EPO,basal} + \dot{E}_{ex}(t) - \frac{1}{t_{1/2}}\ln 2 \cdot E(t), \tag{13}$$

with boundary conditions

$$P(t,0) = R_P E(t), \tag{14}$$

$$M(t,0) = P(t,\mu_F), \tag{15}$$

$$O(t,0) = \frac{1}{k_{Fe}} Fe_{used}, \tag{16}$$

and initial conditions

$$P(0,\mu) = P_0(\mu), \tag{17}$$

$$M(0,\nu) = M_0(\nu), \tag{18}$$

$$O(0,\psi) = O_0(\psi), \tag{19}$$

$$Fe(0) = Fe_0, \tag{20}$$

$$E(0) = E_0. \tag{21}$$

Hemoglobin concentration is a nonlinear function of the amount of iron circulating,

$$Hb(t) = \frac{k_{Fe}\int_0^{\psi_f} O(t,\psi)d\psi}{BV(t)}. \tag{22}$$

Hence, we have a nonlinear coupled system of ordinary and partial differential equations with nontrivial boundary coupling with the following auxiliary equations.

$$\beta_P(E) = \left(\beta_P^{min} - \beta_P^{max}\right) \frac{\left(c_{\beta,P}\right)^{k_{\beta,P}}}{\left(c_{\beta,P}\right)^{k_{\beta,P}} + E^{k_{\beta,P}}} + \beta_P^{max} \tag{23}$$

$$\begin{aligned}\delta_P(E,I) = &\left(\delta_{P,E}^{max} - \delta_{P,E}^{min}\right) \frac{\left(c_{\delta,P,E}\right)^{k_{\delta,P,E}}}{\left(c_{\delta,P,E}\right)^{k_{\delta,P,E}} + E^{k_{\delta,P,E}}} + \delta_{P,E}^{min} \\ &+ \left(\delta_{P,I}^{min} - \delta_{P,I}^{max}\right) \frac{\left(c_{\delta,P,I}\right)^{k_{\delta,P,I}}}{\left(c_{\delta,P,I}\right)^{k_{\delta,P,I}} + I^{k_{\delta,P,I}}} + \delta_{P,I}^{max}\end{aligned} \tag{24}$$

$$\rho_M(E) = \left(\rho_M^{min} - \rho_M^{max}\right) \frac{\left(c_{\rho,M}\right)^{k_{\rho,M}}}{\left(c_{\rho,M}\right)^{k_{\rho,M}} + E^{k_{\rho,M}}} + \rho_M^{max} \tag{25}$$

$$\delta_O(\psi) = \left(\delta_O^{min} - \delta_O^{max}\right) \frac{\left(c_{\delta,O}\right)^{k_{\delta,O}}}{\left(c_{\delta,O}\right)^{k_{\delta,O}} + \psi^{k_{\delta,O}}} + \delta_O^{max} \tag{26}$$

$$f^s(E,I,t) = h_{shift} + \sum_i h(i,I) H_{t_i}^s(t) \tag{27}$$

$$H_{t_i}^s(t) = \frac{1}{1 + e^{-2k_{heavy}(t-t_i)}} \tag{28}$$

$$\rho_{Fe,loss}(Fe) = \begin{cases} \rho_{Fe,const}, & Fe \geq Fe_{th} \\ \rho_{Fe,frac} \cdot Fe, & Fe < Fe_{th} \end{cases} \tag{29}$$

$$\rho_{Fe \to O} = k_{\rho,Fe} Fe_{used} \tag{30}$$

$$Fe_{needed} = k_{Fe} M(t, \nu_f). \tag{31}$$

$$Fe_{avail} = k_{Fe,eff} f(E,I) Fe, \tag{32}$$

$$Fe_{used} = \min\left\{Fe_{needed},\ Fe_{avail}\right\} \tag{33}$$

14 Parameter Value Considerations

- Treatment Protocol:
  We perform simulations for two different "typical" treatment protocols: (1) a patient who goes in for dialysis every third day (ETD) and (2) a patient on a Monday, Wednesday, and Friday (MWF) treatment schedule. In both cases, dialysis is assumed to occur over a four-hour period during which time 5000 units of EPO are assumed to be administered at a constant rate. For those on the ETD schedule, iron is administered every ninth day; those on the the MWF schedule receive iron every Monday. We assume a standard preparation of 62.5 mg iron per administration.

- EPO:
  The half-life $t_{1/2}$ of EPO is estimated to be 25 hours [15]. We assume the rate of EPO produced by the body, $\rho_{EPO,basal}$, is 100 units of EPO per day, chosen to be small relative to the amount provided intravenously.

- Iron: For this set of simulations, we assumed that the net amount of exogenous iron entering the system is equal to the net amount of iron losses in the system. For example, for a patient on MWF treatment schedule, exogenous iron treatment is 62.5 mg of iron every seventh day; therefore we assume that the rate of iron losses to be 62.5/7 mg iron per day.

- Blood volume:
  Typical adult blood volume is between 4.5 and 5 liters. We assume that blood volume reaches its minimum, 4.5 liters, at the end of the four hours of dialysis. For a patient undergoing ETD treatment, we assume blood volume increases linearly to its maximum, 5 liters, just before they start a dialysis treatment. This is also true for a patient on MWF treatment, except that we assume the blood volume increases further, to 5.3 liters, over the weekend.

- Maturity Levels: Based on the literature [6], we assume $\mu_f = 3$ and $\nu_f = 2$. In healthy individuals, red blood cells have an average life span of approximately 120 days. In patients in ESRD, the life span of red blood cells is significantly shorter, so we assume that the *maximum* maturity level in class O is $\psi_f = 120$.

- k_{Fe} : In a healthy individual, each red blood cell (RBC) contains approximately 270 million hemoglobin molecules (CITE). We use basic stoichiometry to determine k_{Fe} as follows:

$$\begin{aligned} k_{Fe} = &\frac{270 \times 10^6 \text{ Hg molecules}}{1 \text{ RBC}} \cdot \frac{10^9 \text{ RBCs}}{1 \text{ billion RBCs}} \cdot \frac{4 \text{ iron atoms}}{1 \text{ Hg molecule}} \\ &\cdot \frac{1 \text{ mol iron}}{6.022 \times 10^{23} \text{ iron atoms}} \cdot \frac{55.845 \text{ grams iron}}{1 \text{ mol iron}} \cdot \frac{10^3 \text{ mg iron}}{1 \text{ gram iron}} \\ = &\, 0.10015 \text{ mg iron / billion RBCs} \end{aligned}$$

- Other parameters: The remaining parameters were given nominal values that produced expected numbers of cells in classes P and M, and appropriate *Hb* concentrations. These parameters could be expected to vary among individuals. The remaining nominal parameter values we use appear in Table 2 in Appendix A.

15 Numerical Solution Methodologies

We solve our system in a sequential manner, beginning with (13). We then solve (9) numerically, using the solution of (13) in the boundary condition, (14). Similarly, use this solution in the boundary condition (15) to solve (10), and we use the solution of (10) when we solve (11) and (12) simultaneously. We solve using Matlab's ode23t solver.

For equations (9), (10) and (11), we use a Galerkin finite element method. We outline this procedure here for class P only, but the same procedure is used for classes M and O.

Let

$$0 = \mu_1 < \mu_2 < \cdots < \mu_{N_P} = \mu_f$$

be a uniform partition of $N_P - 1$ subintervals, each of length $h_P = \frac{\mu_f}{N_P - 1}$. We define N_P piecewise linear continuous functions

$$\phi_j, \quad j = 1, 2, \ldots, N_P,$$

which we will call *trial solution functions*, by

$$\phi_j(\mu) = \begin{cases} \dfrac{\mu - \mu_{j-1}}{h_P}, & \mu_{j-1} \le \mu \le \mu_j, \\ \dfrac{\mu_{j+1} - \mu}{h_P}, & \mu_j \le \mu \le \mu_{j+1}, \\ 0, & \mu < \mu_{j-1} \text{ or } \mu > \mu_{j+1}. \end{cases}$$

We will also use a set of *test functions* $\tilde{\phi}_j$. Typically, the test functions are identically the same as the trial solution functions, but choice of these test functions is discussed later.

We make a weak formulation of (9) by multiplying by the j^{th} test function and integrating over all maturity levels:

$$\int_0^{\mu_f} \frac{\partial}{\partial t} P(t,\mu)\tilde{\phi}_j(\mu)d\mu = -\rho_P \int_0^{\mu_f} \frac{\partial}{\partial \mu} P(t,\mu)\tilde{\phi}_j(\mu)d\mu + \int_0^{\mu_f} \left[\beta_P(E) - \delta_P(E,I)\right] P(t,\mu)\tilde{\phi}_j(\mu)d\mu.$$

We assume that the solution $P(t,\mu)$ has the form

$$P(t,\mu) = \sum_{i=1}^{N_P} a_i(t)\phi_i(\mu), \tag{34}$$

and then manipulate the resulting equation to obtain

$$\begin{aligned}\sum_{i=1}^{N_P} a_i'(t) \int_0^{\mu_f} \phi_i(\mu)\tilde{\phi}_j(\mu)d\mu = & -\rho_P a_{N_P}(t)\phi_j(\mu_f) + \rho_P O(t,0)\phi_j(0) \\ & + \sum_{i=1}^{N_P} a_i(t)\left[\rho_P \int_0^{\mu_f} \phi_i(\mu)\tilde{\phi_j}'(\mu)d\mu \right. \\ & \left. + \left[\beta_P(E) - \delta_P(E,I)\right] \int_0^{\mu_f} \phi_i^A(\mu)\tilde{\phi}_j(\mu)d\mu\right].\end{aligned} \tag{35}$$

We can let j range from 1 to N_P to yield a system of N_P ordinary differential equations for the coefficients $a_i(t)$. We solve this system, and reconstitute our solution using (34).

In order to validate our code, we implement a forcing function strategy. For class P, for example, we solve a modified version of (9):

$$\frac{\partial}{\partial t}\tilde{P}(t,\mu) = -\rho_P \frac{\partial}{\partial \mu}\tilde{P}(t,\mu) + \left[\beta_P(E) - \delta_P(E,I)\right]\tilde{P}(t,\mu) + F(t,\mu). \tag{36}$$

We choose a function such as $\tilde{P}^*(t,\mu) = 10e^{-t/2} + 15e^{-\mu/3}$, which is smooth and decreases to zero with increasing time and maturity level, then determine the forcing function F that guarantees that $\tilde{P}^*$ is the exact solution of (36). We solve (36) numerically and compare our solution with the known exact solution.

It is well known that the solution to (9) will propagate along its characteristic curves, which we can think of as a "wave front." When we use standard linear splines ϕ_j as both the trial solution functions and the test functions, we introduce error at this wave front, which is propagated in time. In Figure 12a, we see that the error can become large and that standard linear splines are insufficient to resolve the solution, as described in [8]. (We will discuss the error that is similar in both Figures 12a and 12b later.)

In order to alleviate this problem, we use a Petrov-Galerkin finite element method, also known as upwinding. We continue using linear spline elements ϕ_j for the trial solution functions, but for the test functions we use second-order functions of the form $\phi_j + \omega\chi_j$, where

$$\chi_j(\mu) = \begin{cases} \dfrac{(\mu - \mu_{j-1})(\mu_j - \mu)}{h^2}, & \mu_{j-1} \le \mu \le \mu_j, \\ -\dfrac{(\mu - \mu_j)(\mu_{j+1} - \mu)}{h^2}, & \mu_j \le \mu \le \mu_{j+1}, \\ 0, & \mu < \mu_{j-1} \text{ or } \mu > \mu_{j+1}. \end{cases}$$

Figure 13 provides an example of standard test elements with varying levels of the upwinding parameter ω. Note that $\omega = 0$ corresponds to no upwinding, or standard linear spline elements.

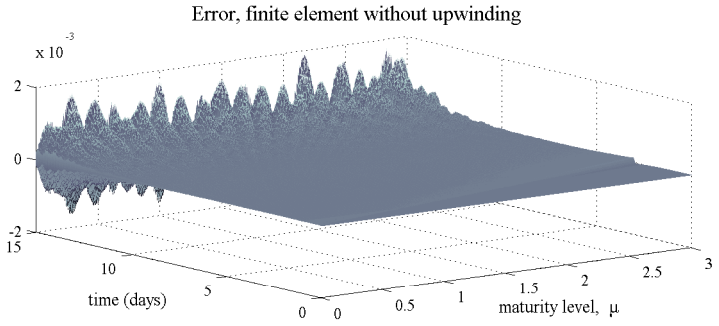

(a)

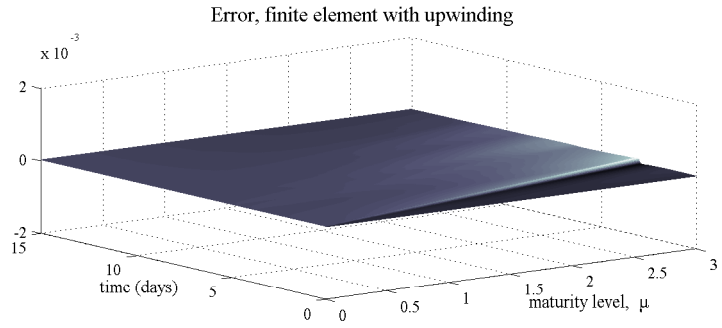

(b)

Figure 12: Error with and without upwinding. Exact solution is of the order 10^2.

When we solve (36) numerically using nonzero values of ω, and compare our solution with the exact solution, we see significant improvement, as in Figure 12b.

We note that the small error seen in both Figure 12a and Figure 12b (that propagates along a linear characteristic from $t = 0$ to approximately $t = 3$) is due to a high order discontinuity between the boundary condition and initial condition at $(t, \mu) = (0, 0)$. This error diminishes with use of a finer mesh on the structure variable.

In order to determine an appropriate value for the parameter ω, we fix the number of elements and solve (36). Figure 14 shows the error using several values for the upwinding parameter.

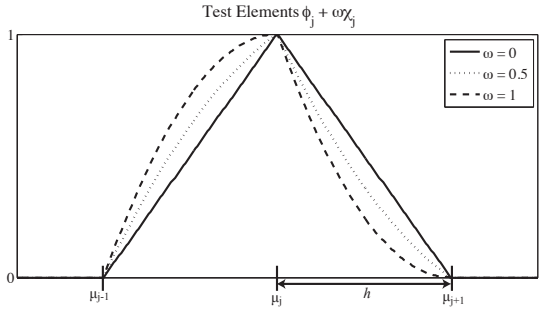

Figure 13: Test basis elements, with varying values of the upwinding parameter ω.

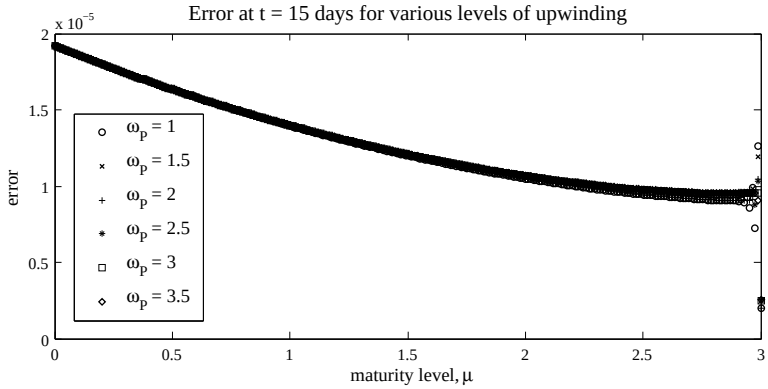

Figure 14: Effect of varying ω_P on error between numerical and exact solution at $t = 15$ for $N = 256$ spatial elements. Exact solution is of the order 10^2.

We note that the error is of the same order for several values of the parameter and we choose to continue our simulations with $\omega_P = 2.5$ as the upwinding parameter for class P.

As one final validation of our code, we sequentially increase the number of splines elements by a factor of two to confirm that the numerical solution converges to the exact solution and to observe the rate of convergence, which is essentially quadratic. The results appear in Table 1.

We repeat this process of validating the code for classes M and O. The results appear in Appendices B and C.

Table 1: Convergence of Solution–Maximum Error at $t = 15$ with $\omega_P = 2.5$ for an increasing number of splines. Exact solution is of the order 10^2.

N_P	Maximum error	(Max Error for N_P)/(Max Error for $2N_P$)
4	0.1298	5.2451
8	0.0247	4.5190
16	0.0055	4.2395
32	0.0013	4.1153
64	3.1384e-04	4.0566
128	7.7365e-05	4.0280
256	1.9207e-05	4.0140
512	4.7850e-06	1.7820
1024	2.6851e-06	

16 Numerical Results and Discussion

An example of our numerical results is shown next for a patient undergoing treatment on the ETD schedule with inflammation level 0.5. As expected, in Figure 15 we see the patient's EPO level

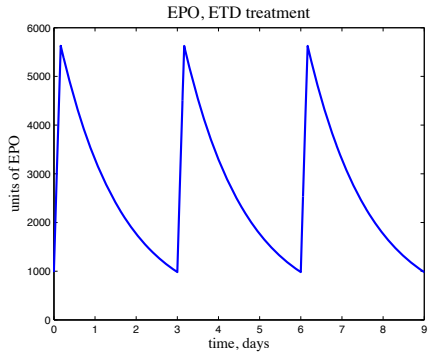

Figure 15: EPO level over time for a patient with inflammation = 0.5 undergoing ETD treatment.

increases every third day when exogenous EPO is provided, and decays between treatments.

In Figure 16, we observe that the boundary condition at $\mu = 0$ for class P mimics the shape of the EPO plot because the recruitment rate is directly proportional to the EPO level.

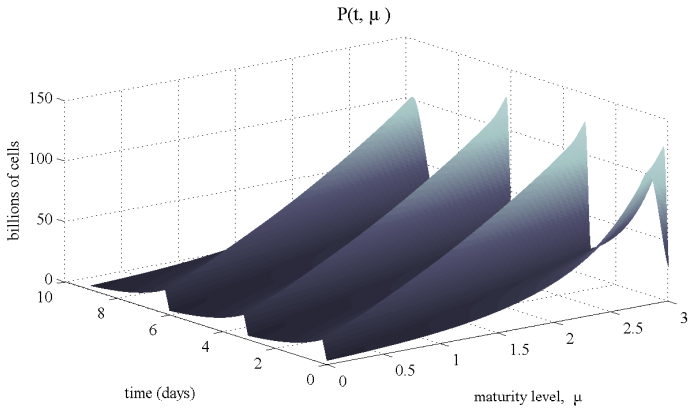

Figure 16: Number of cells in class P for a patient with inflammation = 0.5 undergoing ETD treatment.

Cells in class P mature and divide at a rate of approximately one division per day. Cells in class P mature into class M, which is pictured in Figure 17.

Comparing Figure 16 and 17, we see that, as expected, $P(t, \mu_f) = M(t, 0)$ for all t. Cells in class M divide at a rate of approximately one division per day before they mature into class O.

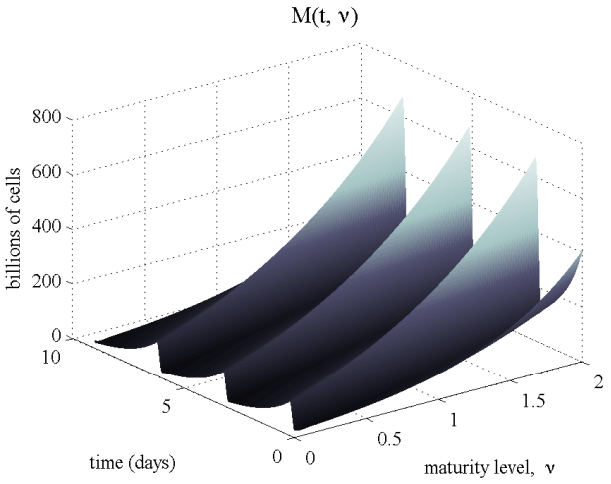

Figure 17: Number of cells in class M for a patient with inflammation = 0.5 undergoing ETD treatment.

As we consider Figure 18, it is worth noting that there has been a change in the time scale. This plot actually closely resembles the plots for classes P and M, but appears much different because results are shown over a time period of 120 days as opposed to just two or three days; this is not an example of the "noise" we discussed previously. The boundary condition, $O(t, 0)$, is not identical to $M(t, \nu_f)$ in Figure 17 because the number of cells maturing in to class O is also dependent on how much iron is available. Note also that cells in class O no longer divide; they simply mature and die.

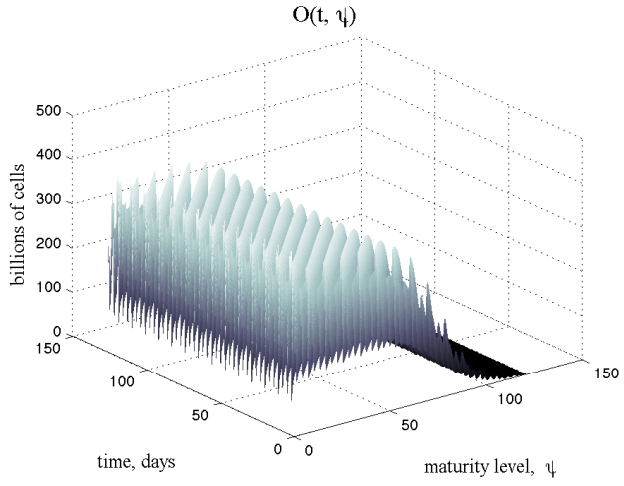

Figure 18: Number of cells in class O for a patient with inflammation = 0.5 undergoing ETD treatment.

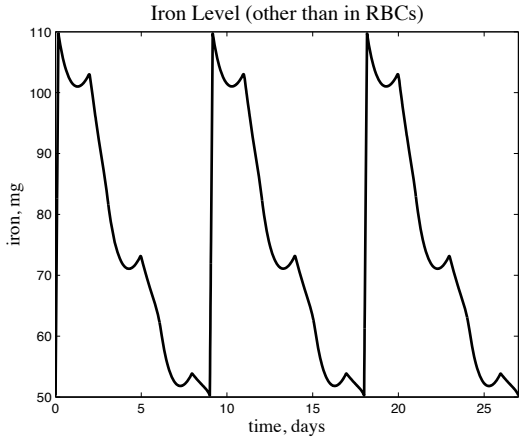

Figure 19: Iron level for a patient with inflammation = 0.5 undergoing ETD treatment.

The amount of iron (other than that being carried in RBCs), in Figure 19, is seen to increase greatly when exogenous iron is introduced (on days 0 and 9). Small increases are due to iron being recycled from RBCs that have died.

Finally, Figure 20 shows the resulting hemoglobin concentration. The desired range, 11 to 13 g/dL, is also shown.

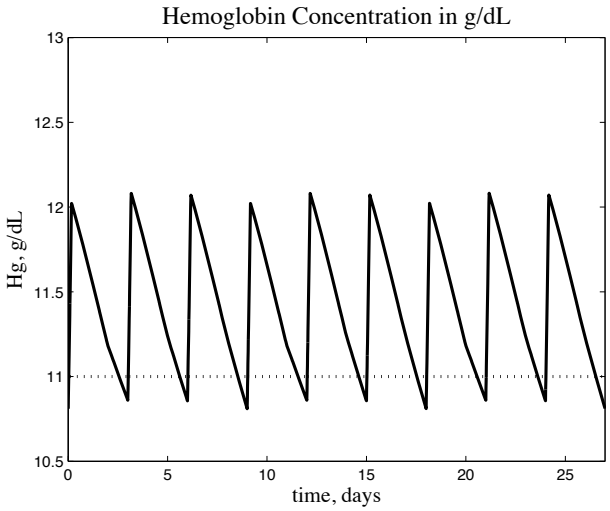

Figure 20: Hemoglobin concentration for a patient with inflammation = 0.5 undergoing ETD treatment.

Figure 21 shows similar results for a patient at inflammation level 0.5 undergoing MWF treatment.

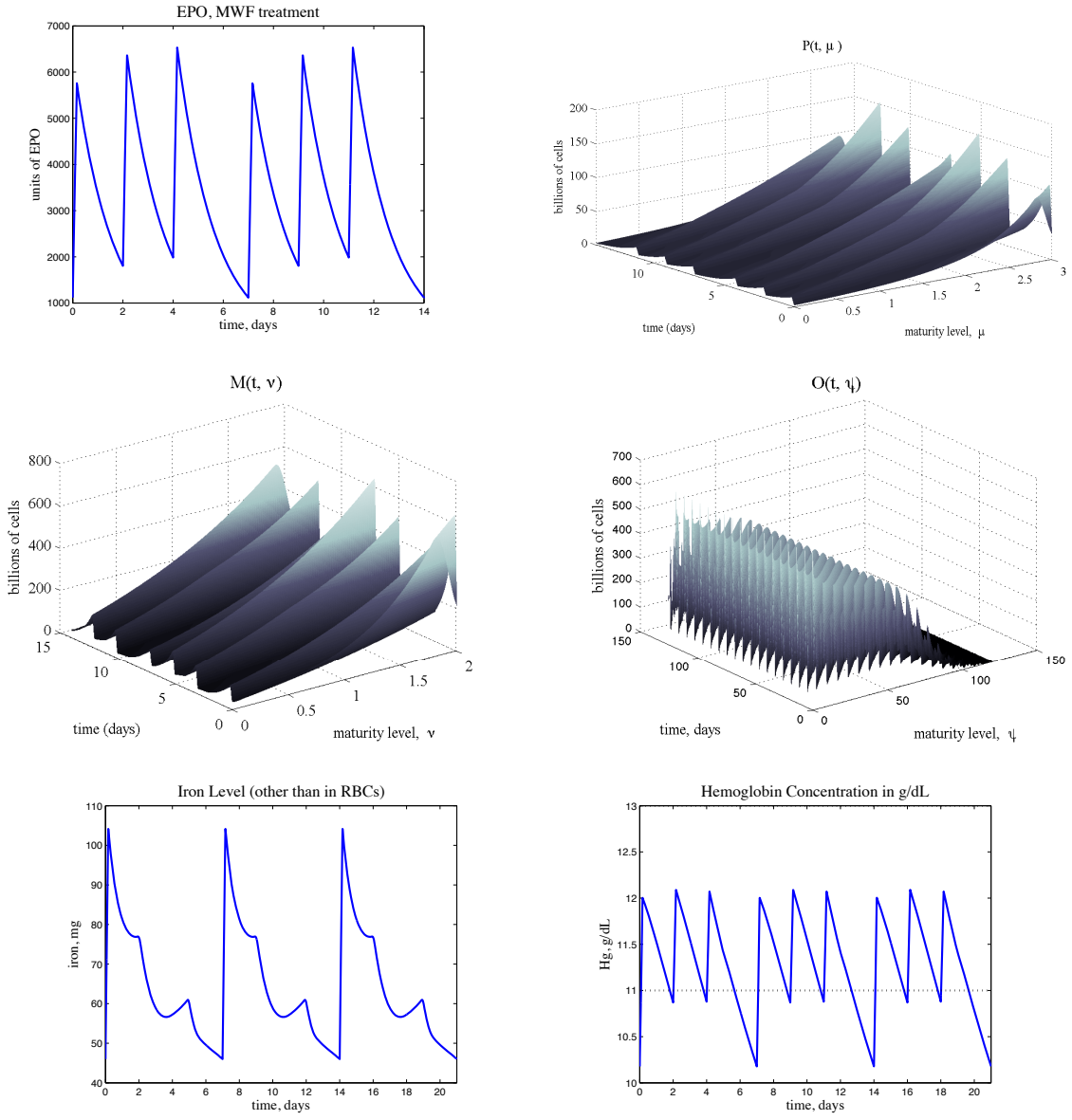

Figure 21

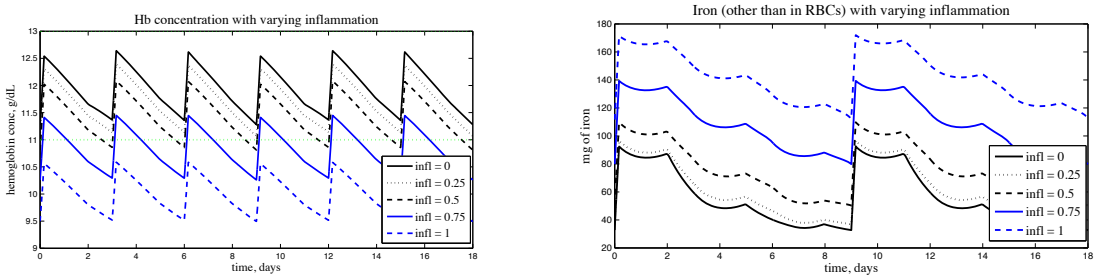

Figure 22: Hemoglobin concentration and iron with varying inflammation, ETD treatment.

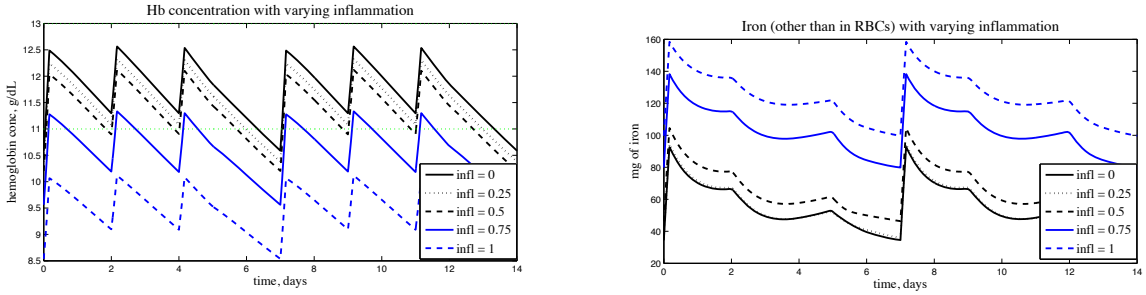

Figure 23: Hemoglobin concentration and iron with varying inflammation, MWF treatment.

We also present some results of varying the inflammation level for both ETD (Figure 22) and MWF treatment (Figure 23).

It should be noted here that the solutions are dependent on the initial conditions, and therefore careful choice of initial conditions must be made in order to produce results that biologically reasonable. For example, if one starts with an an initial condition $O(t, 0)$ that is large, then the iron being carried in those cells eventually ends up in the iron compartment, which in turn affects the recruitment rate into class O. As a result, it is possible, for example, to produce a set of simulations such that the hemoglobin concentration for a patient with inflammation level 0.5 is actually higher than for a patient with a lower inflammation level.

For each treatment protocol, we also compare iron needed, Fe_{needed} and iron available, Fe_{avail}, over time at various levels of inflammation so that we might understand the dynamics of iron in determining the number of cells maturing in to class O (see Figures 24 and 25). It is worth noting again that the solutions (in particular iron available) are dependent on the initial conditions.

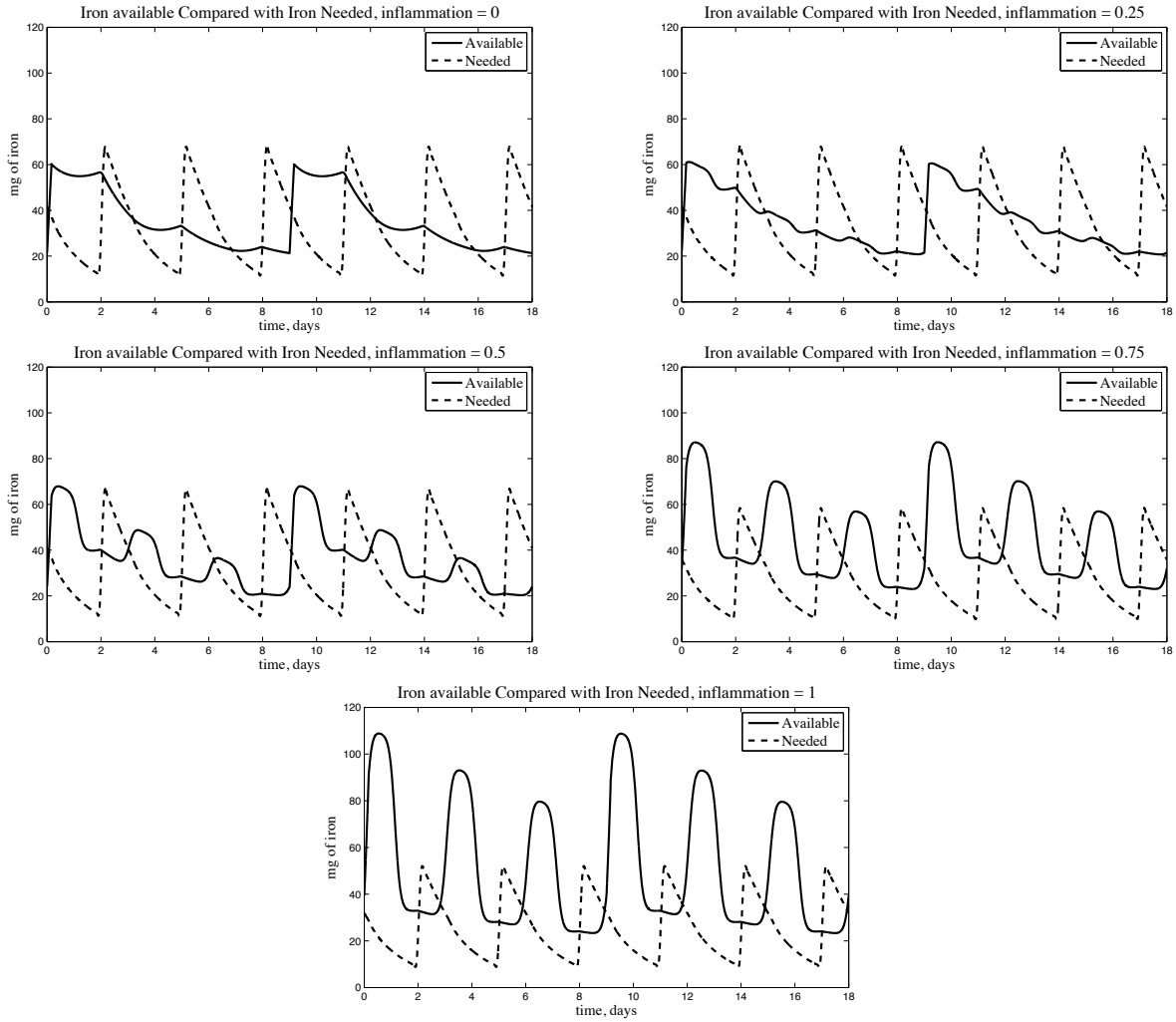

Figure 24: Fe_{needed} and Fe_{avail} with varying inflammation, ETD treatment.

17 Summary

The model presented is capable of describing patients over a broad range of conditions, including various inflammation levels and treatment protocols. Parameter values were prescribed per the literature, when available, and numerical testing validates the use of our code in solving the model. Some numerical results are presented, making note that the results are highly dependent on the initial conditions, which are estimated.

This model makes significant simplifications with regard to how iron is assimilated into red blood cells. As such, the next step will be to revisit the model to determine a more biologically reasonable way to incorporate iron, perhaps through the use of another structure variable which will account for the amount of iron in a cell.

This paper did not attempt to address the concept of iron homeostasis, but it is also becoming more and more evident that understanding iron homeostasis will play a role in this model's ability to predict the outcomes of treatment protocols. It appears that hepcidin production is regulated,

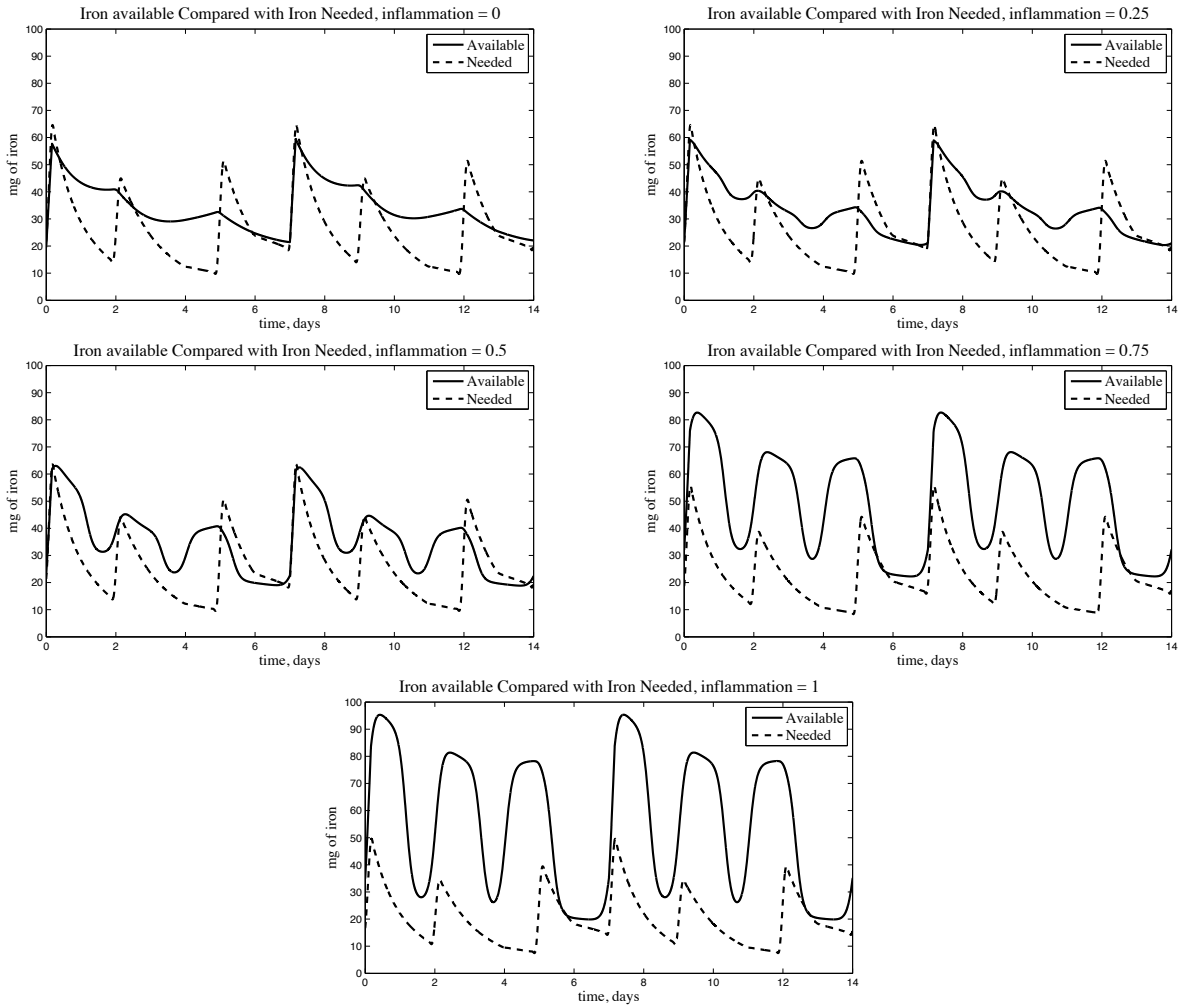

Figure 25: Fe_{needed} and Fe_{avail} with varying inflammation, MWF treatment.

at least in part, by the rate of erythropoiesis [5], but hepcidin has only recently been discovered as the major regulator of iron homeostasis, and therefore its action is only partially understood as the body of literature on hepcidin is relatively small.

This model does address, for the first time, the roles inflammation and iron play in red blood cell dynamics, which are known to have a significant impact on red blood cell dynamics in patients with CKD.

Acknowledgements

This research was supported in part by Grant Number R01AI071915-07 from the National Institute of Allergy and Infectious Diseases.

References

[1] A. Ackleh, K. Deng, K. Ito, and J. Thibodeaux. A structured erythropoiesis model with nonlinear cell maturation velocity and hormone decay rate. *Mathematical Biosciences*, 204(1):21 – 48, 2006.

[2] Suhail Ahmad. *Manual of Clinical Dialysis, Second Edition*. Springer Science + Business Media, LLC, New York, 2009.

[3] H. T. Banks, C. Cole, P. Schlosser, and H. T. Tran. Modeling and optimal regulation of erythropoiesis subject to benzene intoxication. *Mathematical Biosciences and Engineering*, 1(1):15–48, 2004.

[4] J. Belair, M. Mackey, and J. Mahaffy. Age-structured and two-delay models for erythropoiesis. *Mathematical Biosciences*, 128(1-2):317 – 346, 1995.

[5] Tomas Ganz. Iron homeostasis: Fitting the puzzle pieces together. *Cell Metabolism*, 7:288–290, 2008.

[6] L. Israels and E. Israels. Erythropoiesis: an overview. In *Erythropoietins and Erythropoiesis: Molecular, Cellular, Preclinical and Clinical Biology*, pages 3–14. Birkhäuser Verlag, 2003.

[7] W. Jelkmann. Erythropoietin: structure, control of production, and function. *Physiological reviews*, 72(2):449–489, 1992.

[8] Shengtai Li and Linda Petzold. Moving mesh methods with upwinding schemes for time-dependent pdes. *Journal of Computational Physics*, 131:368–377, 1997.

[9] I. Macdougall. Use of recombinant erythropoietins in the setting of renal disease. In S.G. Elliot G. Molineaux, M.A. Foote, editor, *Erythropoietins and Erythropoiesis: Molecular, Cellular, Preclinical and Clinical Biology*, pages 153–159. Birkhäuser Verlag, 2003.

[10] I. Macdougall and A. Cooper. Erythropoietin resistance: the role of inflammation and pro-inflammatory cytokines. *Nephrol. Dial. Transplant.*, 17:39–43, 2002.

[11] J. Mahaffy, J. Belair, and M. Mackey. Hematopoietic model with moving boundary condition and state dependent delay: applications in erythropoiesis. *Journal of Theoretical Biology*, 190(2):135–146, 1998.

[12] R. Means Jr. and S. Krantz. Inhibition of human erythroid colony-forming units by interferons alpha and beta: differing mechanisms despite shared receptor. *Experimental Hematology*, 24(2):204–208, 1996.

[13] National Kidney Foundation Kidney Disease Outcomes Quality Initiative. KDOQI Clinical Practice Guidline and Clinical Practive Recommendations for Anemia in Chronic Kidney Disease: 2007 Update of Hemoglobin Target. *American Journal of Kidney Diseases*, 50(3):471–530, 2007.

[14] R. Ramakrishnan, W. Cheung, M. Wacholtz, N. Minton, and W. Jusko. Pharmacokinetic and pharmacodynamic modeling of human erythropoietin after single and multiple doses in healthy volunteers. *The Journal of Clinical Pharmacology*, 44:991–1002, 2004.

[15] A. Simmons. *Basic Hematology*. Charles C Thomas, Springfield, Illinois, 1973.

[16] P. Stenvinkel. The role of inflammation in the anaemia of end-stage renal disease. *Nephrology, Dialysis, Transplantation*, 16(Suppl 7):36–40, 2001.

[17] U.S. Renal Data System. *USRDS 2008 Annual Data Report: Atlas of Chronic Kidney Disease and End-Stage Renal Disease in the United States*. National Institutes of Health, National Institute of Diabetes and Digestive and Kidney Diseases, Bethesda, MD, 2008.

[18] S. Woo, W. Krzyzanski, and W. Jusko. Pharmacokinetic and pharmacodynamic modeling of recombinant human erythropoietin after intravenous and subcutaneous administration in rats. *Journal of Pharmacology and Experimental Therapeutics*, 319(3):1297–1306, 2006.

Appendices

A Model Parameter Values

Table 2: Model Parameters and Units

Parameter	Units	Parameter value
ρ_P	day^{-1}	1
β_P^{max}	day^{-1}	0.2
β_P^{min}	day^{-1}	0.1
$c_{\beta,P}$	unitless	5250
$k_{\beta,P}$	unitless	5
$\delta_{P,E}^{max}$	day^{-1}	0.03
$\delta_{P,E}^{min}$	day^{-1}	0
$c_{\delta,P,E}$	unitless	1800
$k_{\delta,P,E}$	unitless	6
$\delta_{P,I}^{max}$	day^{-1}	0.05
$\delta_{P,I}^{min}$	day^{-1}	0
$c_{\delta,P,I}$	unitless	0.75
$k_{\delta,P,I}$	unitless	7
R_P	billions of cells/unit EPO	0.018
ρ_M^{max}	day^{-1}	1.2
ρ_M^{min}	day^{-1}	1
$c_{\rho,M}$	unitless	5500
$k_{\rho,M}$	unitless	10
β_M	day^{-1}	0.25
ρ_O	day^{-1}	1
δ_O^{max}	day^{-1}	0.13
δ_O^{min}	day^{-1}	0
$c_{\delta,O}$	unitless	80
$k_{\delta,O}$	unitless	7
$k_{Fe,eff}$	unitless	0.65
f_1	unitless	0.3
$f_{0.5}$	unitless	0.6
k_{heavy}	unitless	5
EPO_{th}	units of EPO	3000
$k_{\rho,Fe}$	day^{-1}	0.993
$\rho_{Fe,frac}$	day^{-1}	0.3
Fe_{th}	mg	15

B Code validation for class M

As in class P, we note that if we don't use upwinding, the error can propagate in time and overwhelm the solution, as demonstrated by comparing the numerical solutions for class M (using the forcing procedure described perviously) with and without upwinding, as in Figures 26a and 26b.

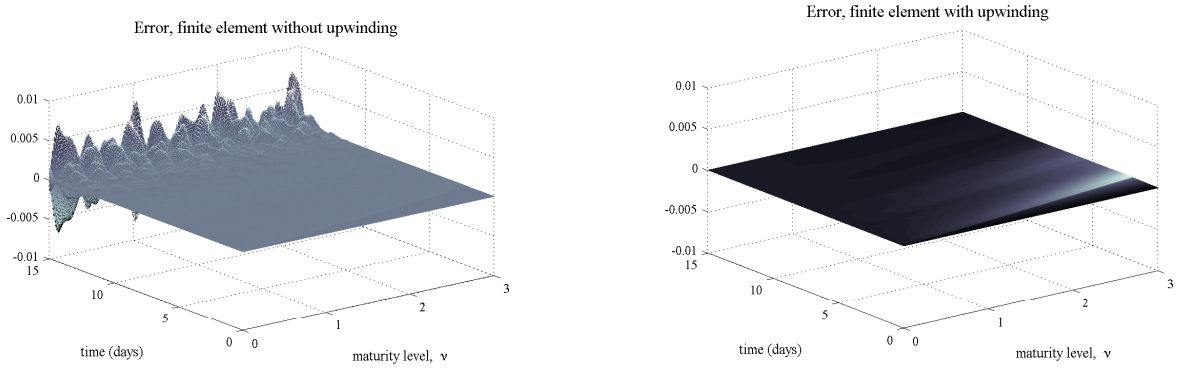

(a) (b)

Figure 26: Error with and without upwinding. Exact solution is of the order 10^2.

In order to determine an appropriate value for the parameter ω_M, we fix the number of elements and compare the error using several values for the upwinding parameter.

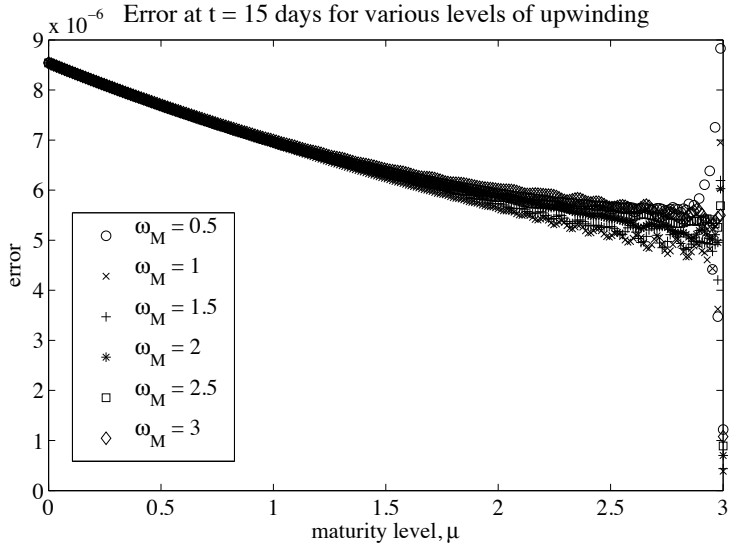

Figure 27: Effect of varying ω_M on error between numerical and exact solution at $t = 15$ for $N = 256$ spatial elements. Exact solution is of the order 10^2.

We note that the error is of the same order for several values of the parameter and we choose to continue our simulations with $\omega_M = 2$ as the upwinding parameter for class M.

As before, we sequentially increase the number of splines elements by a factor of two to confirm that the numerical solution converges to the exact solution. The results appear in Table 3.

Table 3: Convergence of Solution–Maximum Error at $t = 15$ with $\omega_M = 2$ for an increasing number of splines. Exact solution is of the order 10^2.

N_M	Maximum error	(Max Error for N_M)/(Max Error for $2N_M$)
4	0.0614	5.4641
8	0.0112	4.5726
16	0.0025	4.2623
32	5.7693e-04	4.1259
64	1.3983e-04	4.0617
128	3.4427e-05	1.0000
256	3.4427e-05	16.1836
512	2.1273e-06	2.4047
1024	8.8464e-07	

C Code validation for class O

Unlike classes P and M, at time $t = 15$ days, in Figure 28 we are not able to see the error overwhelming the solution without the use of upwinding.

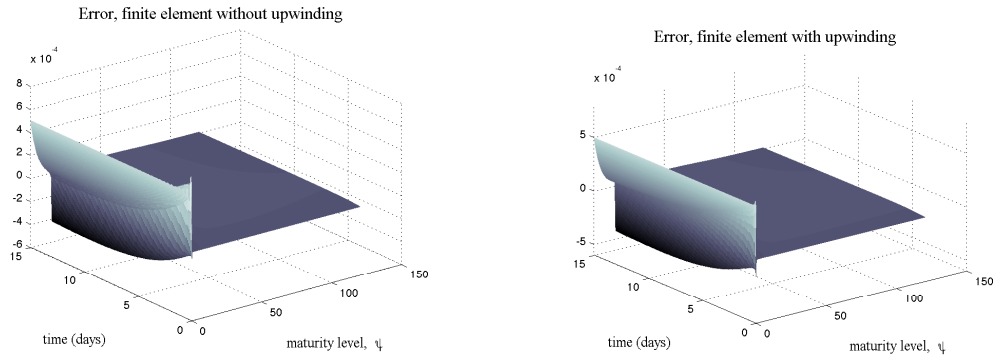

(a) (b)

Figure 28: Error with and without upwinding. Exact solution is of the order 10^2.

It appears there may not be an advantage to using upwinding in this case. We continue investigating by fixing the number of elements and comparing the error using several values of the upwinding parameter ω_O.

We note that the error is of the same order for several values of the parameter, including for no upwinding. We choose to continue our simulations with upwinding (for consistency with the other classes), using $\omega_O = 3.5$ as the upwinding parameter for class O.

As before, we sequentially increase the number of splines elements by a factor of two to confirm that the numerical solution converges to the exact solution. The results appear in Table 4.

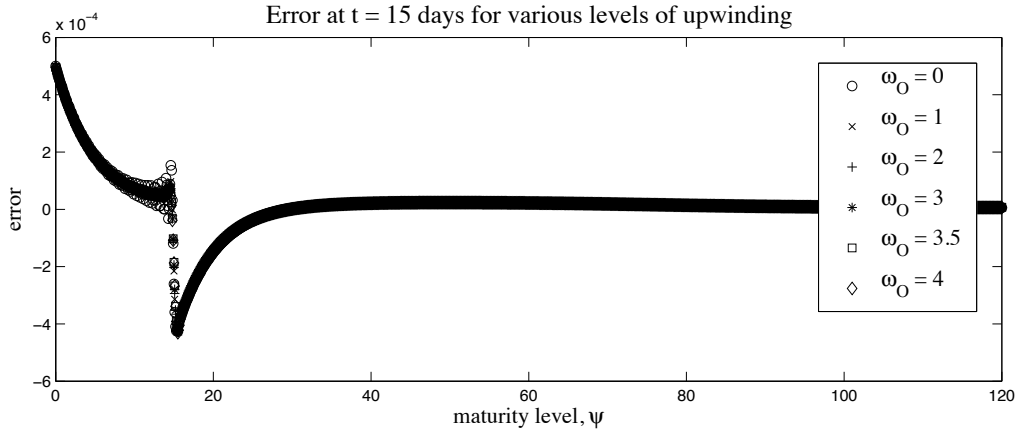

Figure 29: Effect of varying ω_O on error between numerical and exact solution at $t = 15$ for $N = 1201$ spatial elements. Exact solution is of the order 10^2.

Table 4: Convergence of Solution–Maximum Error at $t = 15$ with $\omega_O = 3.5$ for an increasing number of splines. Exact solution is of the order 10^2.

N_M	Maximum error	(Max Error for N_O)/(Max Error for $2N_O$)
8	4.6086	2.6825
16	1.7180	3.1906
32	0.5385	3.5164
64	0.1531	3.7385
128	0.0410	3.8632
256	0.0106	3.9299
512	0.0027	3.9645
1024	6.8052e-04	3.9821
2048	1.7089e-04	3.9911
4096	4.2819e-05	